EPJ Web of Conferences **206**, 06003 (2019) https://doi.org/10.1051/epjconf/201920606003
ISMD 2018

The elastic differential pp cross-section at 13 TeV: an empirical model analysis

Agnes Grau[1,*], *Simone* Pacetti[2,**], *Giulia* Pancheri[3,***], and *Yogendra N.* Srivastava[2,****]

[1]Departamento de Fisica Teorica y del Cosmos, Universidad de Granada, 18071 Granada, Spain
[2]Dipartimento di Fisica e Geologia, Universita' di Perugia, Perugia, Italy
[3]INFN Frascati National Laboratory, Via Enrico Fermi 40, Frascati, Italy 00444

Abstract. We discuss the differential elastic pp cross-section data measured at 13 TeV, through the Coulomb Nuclear Interference region until past the dip. We show that data are consistent with the asymptotic predictions from an empirical model and examine the presence of a zero for the real part of the elastic amplitude near the Coulomb region, well before the dip.

1 Introduction

The TOTEM group has produced a remarkably precise determination of the proton-proton elastic nuclear amplitude at LHC energies [1–4]. In particular, through the Coulomb nuclear interference (CNI) at very small momentum transfer, TOTEM has reported direct measurements of the ρ parameter (that is, the ratio of the real to the imaginary part of the nuclear amplitude in the forward direction at $\sqrt{s} = 8$ &13 TeV. Thus, we now have data for the modulus (through the elastic differential cross-section) and the phase (through CNI) of the near forward nuclear amplitude. In a recent paper[5], we have analyzed the CNI region thoroughly pointing out certain subtleties involved in extracting a value of ρ. We shall elaborate upon it later in the present paper.

The unexpectedly low value of $\rho \sim (0.9 \div 0.1)$ measured by TOTEM at 13 TeV, have pointed to a possible "anomaly": If the Froissart limit is indeed saturated, that is if $\sigma_{tot}(s) \sim L^2(s)$ for large $L >> 1$, where $L = ln(s/s_o)$, then Khuri-Kinoshita theorem[6] forces $\rho(s) \sim \pi/L(s)$. Thus, we expect, $\rho \sim 0.165$ at 13 TeV, quite a bit larger than the TOTEM value. We assume $s_0 = 1\ GeV^2$, in the analysis presented here, following the old convention of early asymptotic particle physics and the scale here is not a free parameter.

There are apparently two ways out of the above dilemma[4]:

- 1. *The Froissart limit is not saturated.* That is, if the rise is fractal -less than quadratic- in L, then ρ still decreases linearly as $[1/L]$, but the coefficient is smaller[7]. More precisely:

$$\text{If } \sigma_{tot}(s) \sim\ L(s)^{1/p} \text{ for } L >> 1;\ [1/2 \le p < 1];$$
$$\Longrightarrow\ \rho(s) = \Big[\frac{\pi}{(2p) \times L(s)}\Big]. \tag{1}$$

*e-mail: igrau@ugr.es
**e-mail: simone.pacetti@pg.infn.it
***e-mail: pancheri@lnf.infn.it
****e-mail: Yogendra.srivastava@gmail.com

For example, if

$$p = 2/3: \ \sigma_{tot} \sim L^{3/2}; \ \rho \sim [\frac{3\pi}{4L}];$$
$$\implies \rho \approx \ 0.124 \ @ \ \sqrt{s} = 13 \ TeV. \tag{2}$$

- 2. *There is a sizeable $C = -1$ contribution even at asymptotic energies*. In QCD language, it is usually interpreted as follows. The leading exchange for hadronic (color singlet) scatterings is provided by the simplest $C = +1$ entity provided by two gluons in a color singlet state. The next step is a $C = -1$ exchange provided by three gluons in a color singlet state[8, 9]. The latter are called odderons and they have been carefully catalogued and analyzed by Block in his review[10]. The near equality of high energy particle-particle and particle-antiparticle total cross-sections confirms the naive belief that the leading term is indeed through the $C = +1$ term. The presence or absence of the $C = -1$ component has generated much controversy in the past. Naturally, the old debate has been considerably fuelled by the recent TOTEM data.

2 The asymptotic empirical model for the differential elastic cross-section

In our previous work [11], we had found that the LHC data @ 8 TeV could be well described by a modified version of the original Barger and Phillips model [12]. In this contribution, we shall apply the above model to the differential scattering data@ 13 TeV presented at the LHCC Meeting in May 2018 [13].

Let the elastic amplitude $\mathscr{A}(s,t)$ be related to the total cross-section as

$$\sigma_{\rm tot}(s) = 4\sqrt{\pi}\,{\rm Im}\left(\mathscr{A}(s,0)\right), \tag{3}$$

so that the elastic differential cross-section reads

$$\frac{d\sigma}{dt}(s,t) = |\mathscr{A}(s,t)|^2 . \tag{4}$$

The amplitude of our modified BP model is [11]

$$\mathscr{A}(s,t) = i\left[F^2(t,t_0)\,\sqrt{A}\,e^{Bt/2} + e^{i\phi}\,\sqrt{C}\,e^{Dt/2}\right]. \tag{5}$$

In Fagundes *et al.* [11], the energy dependence of the parameters was discussed on the basis of asymptotic theorems, as follows.

- The s-dependence of A was chosen so as to satisfy the Froissart bound, as a polynomial in $L(s)$, with coefficients determined by fits to the proton-proton scattering data from ISR to LHC7 :

$$4\sqrt{\pi A(s)} = \left(0.398\,L^2(s) - 3.80\,L(s) + 47.8\right)\ {\rm mb};\ L(s) = \ln(s/s_0), \quad s_0 \equiv 1\,{\rm GeV}^2 . \tag{6}$$

- The s-dependence of the C term is more complicated due to its large variation from low to high energies. A function of $L(s)$ was phenomenologically determined , choosing an asymptotically constant C, with coefficients obtained from the fits as in the case of $\sqrt{A(s)}$, namely

$$4\sqrt{\pi C(s)} = \frac{9.60 - 1.80\,L(s) + 0.01\,L^3(s)}{1.200 + 0.001\,L^3(s)}{\rm mb}. \tag{7}$$

- The proton form factor was defined in terms of the standard dipole expression

$$F(t,t_0) = \frac{1}{(1-t/t_0(s))^2}\,. \tag{8}$$

- While the phase ϕ, introduced in Eq. (5), is very slowly varying through the energy range from ISR to LHC7, the value of the pole $t_0(s)$ of the form factor shows a not negligible dependence on the energy, as it is shown in Fig. 3 of Ref. [11]. However, for large values of s, it tends to the usual value of 0.71 GeV^2. Hence, for high energies, we had frozen both, phase and pole position, as

$$\phi = 2.74\,, \quad t_0 = 0.71 \text{ GeV}^2\,. \tag{9}$$

- As for the two slope parameters in the model, we parametrized them on the basis of on two asymptotic sum rules [14], which were shown to be almost saturated at $\sqrt{s} = 7$ TeV [11], namely we proposed

$$B(s) = \left(0.028\, L^2(s) - 0.230\right) \text{ GeV}^{-2};\; D(s) = (0.29\, L(s) - 0.41) \text{ GeV}^{-2} \tag{10}$$

We stress that the asymptotic behaviour of the slope $B(s)$ chosen above, differs from the usual $\ln(s)$ behaviour expected from Regge or Pomeron pole trajectories. Namely, in this empirical model, the slope in the forward region increases faster than a logarithm, in agreement with an earlier study by Ryskin and Shegelsky [15],[see, also [16], [17], [18] and predicting a higher energy behaviour as confirmed by the recent TOTEM observations at LHC13.

In the following subsections, we shall apply this model to the recent TOTEM data, starting with the CNI region.

2.1 The Coulomb interference region

In a recent paper [5], we have presented results for the CNI region at 8 and 13 TeV from the empirical model described above. The basic observation following from this model and relevant to the study of the ρ parameter, is that besides the well-known *diffraction dip* due to a zero in the absorptive part of the amplitude, there is also a zero in the real part of the nuclear amplitude [19]. What is important here is that at LHC energies, the real part vanishes in the CNI region thereby complicating the extraction of the ρ parameter.

For a phenomenological analysis of the CNI region involving small momentum transfer t, we use Eq. (17) of Ref. [4], where an amplitude $\mathscr{A}^G(s,t)$ is defined that has the standard nuclear amplitude $\mathscr{A}(s,t)$, as described above, times an order-α complex phase $\sim \alpha G(s,t)$, with respect to the real Coulomb amplitude. Explicitly:

$$\mathscr{A}^G(s,t) = \mathscr{A}(s,t)\Big(1 - i\alpha G(s,t)\Big) \tag{11}$$

where

$$G(s,t) = \int_{-s+4m^2}^{0} (dt')\Big[ln(\frac{t'}{t})[\frac{dF^2(t')}{dt'}] - \Big(\frac{\mathscr{A}(s,t')}{\mathscr{A}(s,t)} - 1\Big)\frac{I(t,t')}{2\pi}\Big];$$
$$I(t,t') = \int_0^{2\pi} \frac{F^2[t+t'+2\sqrt{tt'}\cos(\phi)]}{t+t'+2\sqrt{tt'}\cos(\phi)} d\phi\,. \tag{12}$$

The complete elastic differential cross-section is defined as

$$\frac{d\sigma}{dt}(s,t) = \Big|\mathscr{A}^G(s,t) + \mathscr{A}^C(s,t)\Big|^2, \tag{13}$$

where $\mathscr{A}^c(s,t)$ is the Coulomb amplitude, defined in terms of the electromagnetic form factor, as

$$\mathscr{A}^C(s,t) = \frac{2\sqrt{\pi}\,\alpha}{t} F^2(t);$$
$$F(t) = \frac{1}{[1-\frac{t}{0.71\ GeV^2}]^2} \tag{14}$$

As stated earlier, the CNI has been measured with great precision by the TOTEM group at 8 and 13 TeV. Numerical values of the elastic differential cross-section for the momentum transfer region 8.8×10^{-4} GeV^2 $< |t| <$ 0.1 GeV^2, for the 8 TeV data are presented in Table 3 of Ref. [2] and for the 13 TeV data in Table III of Ref. [4].
To isolate CNI, TOTEM [4] shows the 13 TeV data in the following way:

1. in their Fig. 14 covering momentum transfer up to $|t| \leq 0.15$ GeV^2.
2. In their Fig. 15 up to $|t| \leq 0.07$ GeV^2.
3. A fractional quantity $\mathscr{X}$ is plotted using differential cross-section data up to $|t| \leq 0.15$ GeV^2, after subtracting from it a reference term formed from the sum of the purely nuclear and Coulomb differential cross-sections.

Explicitly

$$\mathscr{X}(s,t) = \frac{[d\sigma/dt]_{\rm data} - {\rm Ref}_4(s,t)}{{\rm Ref}_4(s,t)}, \tag{15}$$

where the reference value at $\sqrt{s} = 13$ TeV is defined as in Ref.[4], i.e.,

$${\rm Ref}_4(s_{13},t) = 633(mbGeV^{-2})\ e^{20.4\ t/GeV^2} + [\frac{d\sigma}{dt}]_C, \tag{16}$$

is the sum of the exponential fit and the Coulomb cross-section

$$[\frac{d\sigma}{dt}]_C = \left|\mathscr{A}^C(s,t)\right|^2, \tag{17}$$

where the Coulomb amplitude $\mathscr{A}^C(s,t)$, defined in Eq. (14), is *negative*.
In the CNI region, TOTEM [4] uses the following parametrization for the nuclear amplitude, called $\mathscr{A}^N$,

$$\mathscr{A}^N(s,t) = |\mathscr{A}^N(s,t)|e^{i\Phi(s,t)};$$
$$|\mathscr{A}^N(s,t)| = \sqrt{a}\ exp[\frac{1}{2}\sum_{n=1}^{N_b} b_n t^n];$$
$$\Phi(s,t) = \frac{\pi}{2} - \tan^{-1}\rho(s,t) = [\text{Constant}]. \tag{18}$$

In the above, b_1 is the "large" diffraction slope and $b_{2,3}$ are supposed to account for minor fluctuations in the low-t data. It is interesting to note that for the data in Ref. [4] covering a smaller t-interval, $|t|_{\rm max} = 0.07$ GeV^2, for $N_b = 1$, 2, 3, the χ^2 per degree of freedom, $\bar{\chi}^2$, have roughly the same value: $\bar{\chi}^2 = 0.7, 0.6, 0.6$, respectively; whereas data that cover a larger t-interval, $|t|_{\rm max} = 0.15$ GeV^2, the fit with just one term $N_b = 1$ has a much larger $\bar{\chi}^2 = 2.6$ compared to $\bar{\chi}^2 = 1.0$ for $N_b = 2$ and $\bar{\chi}^2 = 0.9$ for $N_b = 3$. In fact, as the authors of Ref. [4] note themselves, the quality of fit is bad and no values for ρ are displayed for $N_b = 1$ and

$|t|_{\max} = 0.15$ GeV^2. As we shall see below, this is due to their chosen parametrization of the nuclear amplitude in Eq. (18). For example, the form of the nuclear amplitude adopted in Eq. (18),with ρ assumed constant, leaves no room for the real part of the nuclear amplitude to vanish near the CNI region, whereas our model does.
Using the model of Eq. 5, with the asymptotics as discussed above, we now define 4-sets of *rotated* amplitudes through the following substitution possibilities. For further details, see [5]. We have considered all four possibilities with the following four sets of nuclear amplitudes:

$$\begin{aligned} s \to se^{-i\pi/2}; ln(s) \to ln(se^{-i\pi/2}) = ln(s) - i\pi/2; \\ j=0: \ \mathscr{A}_0(s,t) : \text{no rotation at all}; \\ j=1: \ \mathscr{A}_1(s,t) : \text{only } A(s) \to A(se^{-i\pi/2}) \ \& \ C(s) \to C(se^{-i\pi/2}) \text{ rotated}; \\ [\text{no rotation of the phases}] \ B \ \& \ D; \\ j=2: \ \mathscr{A}_2(s,t) = \mathscr{A}(se^{-i\pi/2},t); \ \text{complete rotation}; \\ j=3: \ \mathscr{A}_3(s,t) = \frac{1}{2}\left[\mathscr{A}(s,t) + \mathscr{A}\left(se^{-i\pi},t\right)\right]; (s \Leftrightarrow u \text{ symmetric}) \end{aligned} \tag{19}$$

The j-th differential cross-section is obtained as

$$\frac{d\sigma_j}{dt}(s,t) = \left|\mathscr{A}_j(s,t) + \mathscr{A}^C(s,t)\right|^2; \tag{20}$$

where the nuclear j-th and Coulomb amplitudes are given in Eq. (19) and (14) respectively, and residuals for the two data sets at $\sqrt{s} = 8$ TeV and 13 TeV,

$$\left\{ t_k, \frac{d\sigma}{dt}(s,t_k)_{\text{data}}, \delta\left[\frac{d\sigma}{dt}(s,t_k)_{\text{data}}\right] \right\}_{k=1}^{M(s)}, \tag{21}$$

are defined as

$$R_j(s,t_k) = \frac{\frac{d\sigma}{dt}(s,t_k)_{\text{data}} - \frac{d\sigma_j}{dt}(s,t_k)}{\frac{d\sigma_j}{dt}(s,t_k)}, \qquad \begin{aligned} s &= s_8, s_{13}, \\ j &= 0,1,2,3, \\ k &= 1,\ldots,M(s). \end{aligned} \tag{22}$$

As one can see in Fig.(1), the agreement with data is excellent for the nuclear amplitudes $\mathscr{A}_{1,2,3}(s,t)$ (red, green, blue areas and lines), whereas $\mathscr{A}_0$ (black area and line) is essentially ruled out. The corresponding residuals $R_{1,2,3}(s,t)$ both at $\sqrt{s} = 8$ and 13 TeV are practically zero all the way up to $|t|_{\max} = 0.2$ GeV^2.

It was shown in[5] that both the real and imaginary parts of the nuclear amplitude are practically identical for $\mathscr{A}_2$ and $\mathscr{A}_3$, but they are substantially different from $\mathscr{A}_o$ and $\mathscr{A}_1$. Moreover, the predictions from the amplitudes $\mathscr{A}_2$ and $\mathscr{A}_3$ are in remarkable accord with the TOTEM data in the CNI region whereas those from $\mathscr{A}_o$ and $\mathscr{A}_1$ are decidedly inferior. We used the values of the parameters from[11] for the four nuclear amplitudes. Hence, these are *predictions* for the absolute differential cross-section near the forward region at 8 and 13 TeV.

2.2 ρ and mean $\bar{\rho}$

TOTEM assumes that ρ is a constant and uses CNI data over $0 \le |t| \le |t|_{max}$ (with $|t|_{max} =$ 0.07&0.15 GeV^2) to extract a value for ρ @ 8 & 13 TeV. On the other hand, if there is a zero in the real part of the nuclear amplitude within or nearby the CNI region [*vedi* Sec(2.1)],

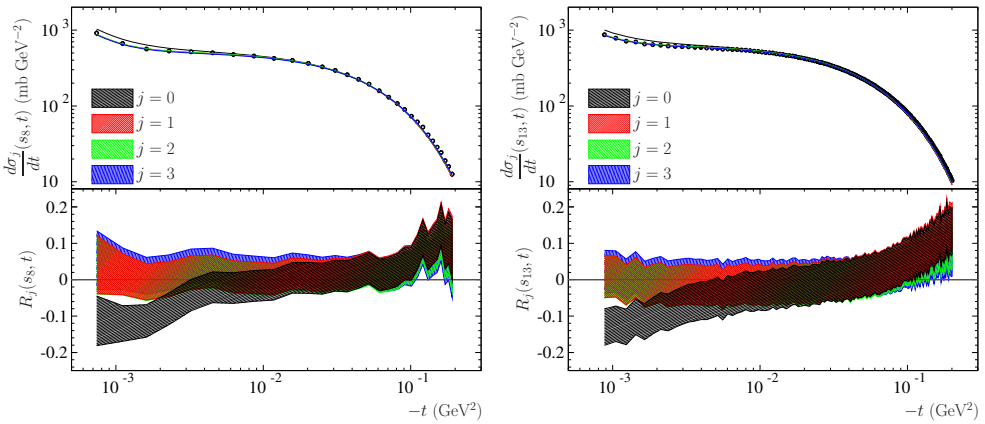

Figure 1. Model analysis of TOTEM data in the small $-t$ region, at $\sqrt{s} = 8$ and 13 TeV, in left and right figures. Upper panel: Data on the differential cross-section and superimposed the predictions corresponding to the parametrisations of the nuclear amplitude given in Eq. (19). Lower panel: residuals as defined in Eq. (22).

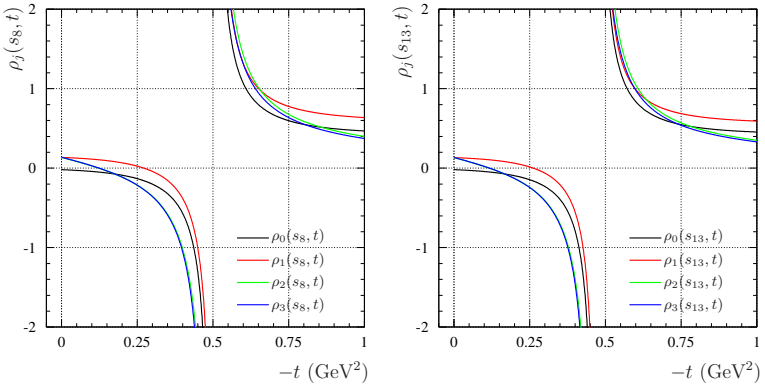

Figure 2. The $\rho(s,t)$ values at 8 (left), 13 TeV (right) from the rotated mBP2 model described in the text.

this would influence the extraction of ρ, as one can see from Fig. 2. $\rho(s,t)$ for our preferred solutions $j = 2,3$. indeed have a zero around $t = -0.15\ GeV^2$ for 8 & 13 TeV. We construct an average $[\bar{\rho}]$ over a t region, that can be compared to the TOTEM ρ that is assumed constant:

$$\bar{\rho}_j(s,t) \equiv \frac{\int_t^o (dt)\rho(s,t)_j (d\sigma/dt)_j}{\int_t^o (dT)(d\sigma/dt)_j};\ (j = 0,1,2,3). \tag{23}$$

These are shown in Fig.(3). It is satisfactory that while $\rho_{2,3} = 0.133$, $\bar{\rho}_{2,3}(0 \leq |t| \leq 0.15\ GeV^2) \approx 0.09$ at 13 TeV, remarkably close to the value $[0.09 \pm 0.01]$ found by TOTEM for ρ *assumed to be a constant in this t-interval*. This bolsters our confidence in that the real part does possess a zero near the CNI region. Further evidence for such a zero in the real part -at a smaller $|t|$ value than where the zero for the imaginary part lies- also follows from geometrical scaling[19].

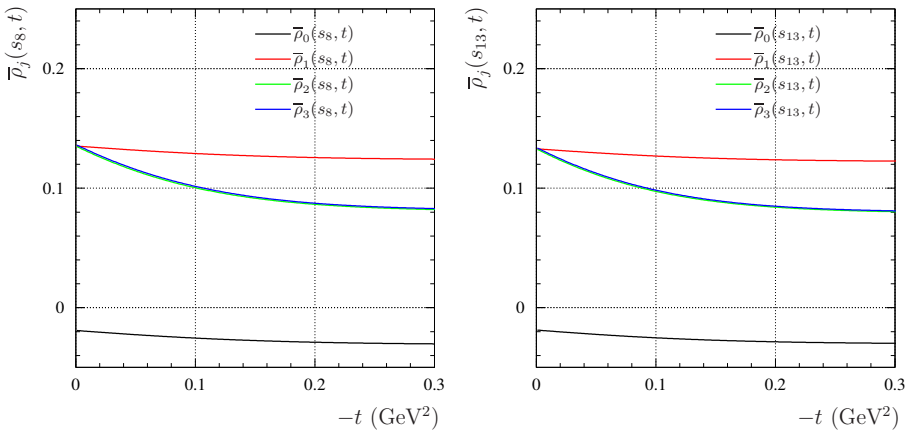

Figure 3. Mean values of $\rho_j(s,t)$ at 8 and 13 TeV

2.3 The structure outside the Coulomb region

We have seen in Subsec.(2.2) that the TOTEM data in the CNI region are consistent with the empirical model if crossing symmetry is implemented in the asymptotic expression for the model constants, what we call the rotated model (in its different versions). However, it leaves moot the question whether the form factor multiplies just the first (A) term of the BP amplitude as discussed above, called mBP2, or both (A & C) terms as in the model labelled as mBP2-1 and discussed in the Appendix of [11], where it was also pointed out that both versions of the model would give good fits to the data from ISR to 7 TeV. We show in the left panel of Fig. 4 the application to the 13 TeV TOTEM data in the full $-t$ range, of model mBP2 in both the rotated and unrotated version. The value of the parameters follows the parametrization in Eqs.(5-10). The result is shown in the left panel and indicates that, while the small $-t$ behaviour is satisfactorily reproduced, the model fails both at the dip and beyond.

Given the simplicity of the empirical model, it is worth inquiring further about its applicability to present and future LHC high-t data. it We illustrate it by presenting a free parameter fit to the 13 TeV data where (i) both (A & C terms) are multiplied by the form factor [as in the model labelled mBP2-1]; (ii) no additional phase between Coulomb and nuclear amplitudes is assumed [as in Eq.(20)]. Explicitly, we have used the following expression: :

$$\frac{d\sigma}{dt} = |\mathscr{A}(s,t) + \frac{2\sqrt{\pi}\alpha}{t}\frac{1}{(1-\frac{t}{0.71\ GeV^2})^4}\frac{1}{\sqrt{2.56819}}|^2;$$
$$\Re e\mathscr{A}(s,t) = \frac{1}{(1+|t|/t_0)^4}\{[\rho(\sqrt{A}+\sqrt{C}\cos\phi)+\sqrt{C}\sin\phi)]e^{B(s)t/2} - \sqrt{C}\sin\phi e^{D(s)t/2}\};$$
$$\Im m\mathscr{A}(s,t) = \frac{1}{(1+|t|/t_0)^4}[\sqrt{A}e^{B(s)t/2} + \sqrt{C}\cos\phi e^{Dt/2}], \tag{24}$$

and fix the value of ρ to the reported experimental value, all the other parameters are let to vary. The result is shown in the right panel of Fig. 4, where the resulting $\chi^2/N_{dof} = 0.838$ indicates that the fit with the form factor factorized outside the full nuclear amplitude can indeed reproduce very well the 13 TeV data.

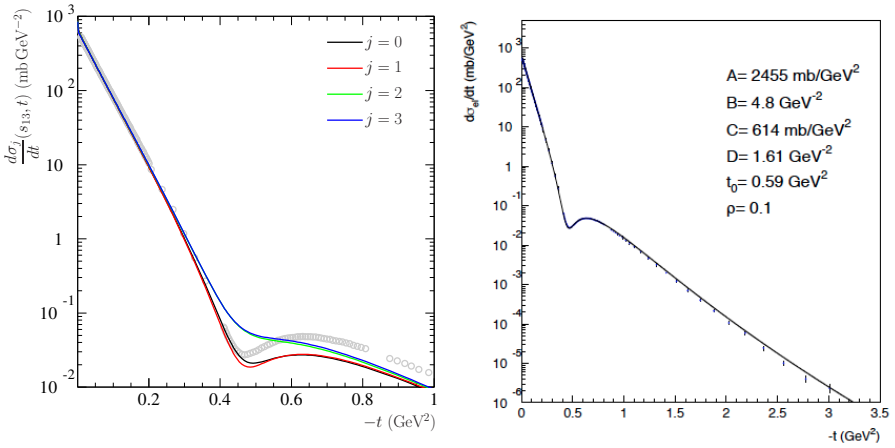

Figure 4. Left panel: application to the 13 TeV TOTEM data, read from [13], of the asymptotic empirical model described in the previous subsection, in the original and in the rotated version using model mBP2 from [11], and $t_0 = 0.71\ GeV^2$. In the right panel, we show a free parameter fit of pp data using the mBP2-1 model with the Form Factor multiplying both terms in the amplitude. The expression used for the free fit includes the Coulomb term, but no additional phase between the Coulomb and the nuclear amplitude. The $\chi^2/dof = 0.838$.

A more complete analysis shall be undertaken when definitive high-t data @ 13 TeV become available.

3 The total cross-sections

We shall include here our analysis of the asymptotic behavior of the total cross-section following a QCD model which explicitly shows that the high energy limit, i.e. saturation of the Froissart bound, has not been reached. In this model, which includes an eikonalized mini-jet cross-section with infrared gluon resummation, the Froissart bound need not be reached. Our model for the total cross-section is built through a one-channel real eikonal function, inclusive of mini-jets to drive the rise and infrared soft gluon resummation to tame it, i.e.

$$\sigma_{total} = 2\int d^2\mathbf{b}[1 - e^{-\bar{n}(b,s)/2}] = 2\int d^2\mathbf{b}[1 - e^{-[\bar{n}_{soft}(b,s)+\bar{n}_{mini-jets}(b,s)]/2}] \tag{25}$$

$$\bar{n}_{soft}(b,s) = A_{FF}(b)\sigma_{soft}(s) = \frac{1}{(2\pi)^2}\int d^2\mathbf{q}e^{i\mathbf{q}\cdot\mathbf{b}}[F_p(\mathbf{q})]^2\sigma_{soft}(s) \tag{26}$$

$$\sigma_{soft}(s) = constant\ or\ slowly\ decreasing\ function \tag{27}$$

$$\bar{n}_{mini-jets}(b,s) = A_{BN}(b,s)\sigma_{mini-jets} = \frac{e^{-h(b,s)}}{\int d^2\mathbf{b}\ e^{-h(b,s)}}\sigma_{mini-jets}(s;p_{tmin},PDF) \tag{28}$$

This model is called *BN model* as its most distinctive feature is given by resummation (down into the $k_t \approx 0$ region) of all the Poisson distributed soft gluons which are emitted during a semi-hard (mini-jet) parton parton collision. The impact parameter distribution of partons in this simplified model is schematically divided into two components, partons which mirror the distribution of partons in each individual proton (through the Fourier transform of the proton form factor) and partons which are correlated to partons in the other proton through semi-hard collisions. This model, recently described in [20], was developed through the

years [21–23], and focuses on the behaviour of the resummed and regularized soft gluon distribution $h(b,s)$. Under the ansatz that the coupling of very soft gluons to their source can be phenomenologically described to be no more singular than k_t^{-2p} with $1/2 < p < 1$, we had been able to show that the total cross-section asymptotically behaves as [23]

$$\sigma_{total} \sim [\ln s]^{1/p} \qquad as \to \infty \tag{29}$$

Thus, since $p > 1/2$, the above limit can satisfy the Froissart bound, although not being close to saturate it yet. In Fig. 5 we show the result of applying this model to present data for the total cross-section, both for pp and $\bar{p}p$. In the figure, the blue band represents the result of the BN model for two types of parton densities, as indicated, and the dotted lines the results from the empirical model described at the beginning of this note.

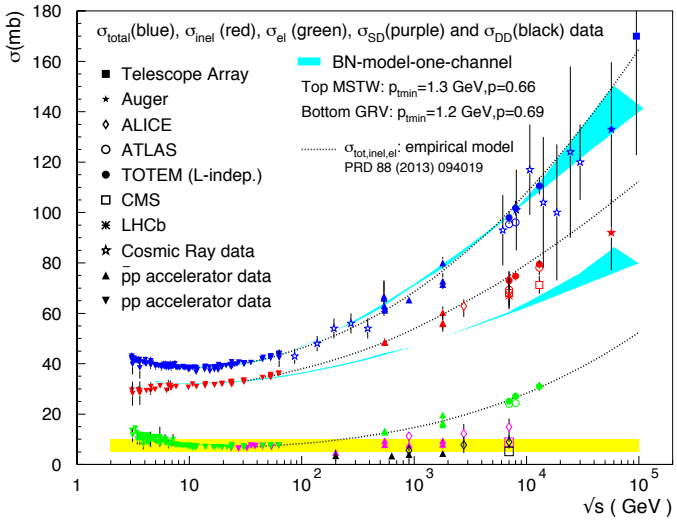

Figure 5. The rise of the total, elastic and inelastic proton proton cross-sections: comparing data with two models described in the text.

We should point out, before concluding this note, that the BN model as described in this section in the one-channel eikonal mini-jet formulation, cannot yet be applied to the description of the differential elastic cross-section. While it gives a good description of the imaginary part of the elastic amplitude at $t = 0$, and hence of the total cross-section, if fails so far in two respects: i) its does not adequately describe the dip structure, and ii) it does not properly separate elastic and diffraction channels, which are usually described in a two-channel formalism. As a consequence, as seen in Fig. 5, the BN does not reproduce the full inelastic cross-section (blue band), but only the contribution to non-diffractive part of the phase space [20]. We are working to understand how to extend the model to clarify these points.

Acnowledgments and conclusions

One of us, G.P., is grateful to the organizers of ISMD 2018 for invitation to the Conference and the kind support. One of us acknowledges hospitality at the MIT Center for Theoretical

Physics, where parts of this contributions were prepared. Both G.P. and Y.S. thank Earle Lomon, from MIT-CTP, for useful and enlightening discussions.

Note added in proof

After this presentation, the TOTEM group has released high-t data at 13 TeV [24].

References

[1] The TOTEM Collaboration, G. Antchev *et al*, *Euro. Phys. Lett*, **96** (2011) 21002.
[2] The TOTEM Collaboration, G. Antchev *et als.*, *Eur Phys. J.* **C76** (2016) 661; arXiv: 1610.00603 [nucl-ex] 3 Oct 2016.
[3] The TOTEM Collaboration, G. Antchev *et als.*, CERN-EP-2017-321, CERN-EP-2017-321-V2; [arXiv:1712.06153 [hep-ex]].
[4] The TOTEM Collaboration, G. Antchev *et als.*, CERN-EP-2017-335, CERN-EP-2017-335-v3;. [arXiv:1812.04732 []hep-ph]]
[5] S. Pacetti, Y. N. Srivastava, G. Pancheri, *Analysis and Implications of precision near-forward TOTEM data*, *Phys. Rev.*, **D99** (2019) 034014;arXiv: 1811.00499 [hep-ph]
[6] N. N. Khuri and T. Kinoshita, *Phys. Rev.*, **B720**,137 (1965); *ibidPhys. Rev.*, **B706**, 140, (1965); *Phys. Rev. Lett.*, **14** (1965) 84.
[7] G. Pancheri and Y. Srivastava, Eur. Phys. J., **C77** (2017) no. 3, 150 arXiv:hep-ph/1610.10038.
[8] K. Kang and B. Nicolescu, *Phys. Rev.*, **D11** (1975) 2461.
[9] E. Martynov and B. Nicolescu, *Phys. Lett.*, **B778** (2018) 414. [arXiv:1711.03288 [hep-ph]].
[10] M. M. Block, *Phys. Rept.*, **436** (2006) 71 [hep-ph/0606215].
[11] D. A. Fagundes, A. Grau, S. Pacetti, G. Pancheri and Y. N. Srivastava, *Phys. Rev.*, **D 88** (2013) 094019 [arXiv:1306.0452 [hep-ph]].
[12] R. J. N. Phillips and V. D. Barger, *Phys.Lett.* **B46** (1973) 412.
[13] https://indico.cern.ch/event/726320/contributions/2988542/attachments/1658309/2656234/FRavera_LHCC_30May2018.pdf
[14] G. Pancheri, Y. Srivastava and N. Staffolani, Acta Phys. Polon. B **36** (2005) 749 [hep-ph/0411007].
[15] V. A. Schegelsky and M. G. Ryskin, Phys. Rev. D **85** (2012) 094024 doi:10.1103/PhysRevD.85.094024 [arXiv:1112.3243 [hep-ph]].
[16] V. Okorokov, *Advances in High Energy Physics* (2015) 914170 ; arXiv:1501.01142.
[17] L. Jenkovszky, *et. al*, *EPJ* **A 54**, 116 (2018) 116.
[18] E. Ferreira, A. K. Kohara and J. Sesma, *Phys.Rev.* **D98** (2018) 094029.
[19] A. Martin, *Phys. Lett.*, **B 404**, 137 (1997)
[20] D. A. Fagundes, A. Grau, G. Pancheri, O. Shekhovtsova, Y. N. Srivastava, Phys.Rev. D96 (2017) no.5, 054010.
[21] A. Corsetti, A. Grau,, G. Pancheri (Frascati), Y.N. Srivastava, Phys.Lett. **B382** (1996) 282-288.
[22] A. Grau, G. Pancheri, Y.N. Srivastava, Phys.Rev. **D60** (1999) 114020.
[23] A. Grau, Rohini M. Godbole, Giulia Pancheri, Yogendra N. Srivastava, Phys.Lett. **B682** (2009) 55-60.
[24] The TOTEM Collaboration, G. Antchev *et als.*, CERN-EP-2018-338, TOTEM-2018-003; [arXiv:1812.08283 [hep-ph]].